Unmixing of Spectral Components Affecting AVIRIS Imagery of Tampa Bay

Kendall 1. Carder, Z.P. Lee, Robert F. Chen

University of South Florida
Department of Marine Science
140 Seventh Avenue South
St. Petersburg, FL 3370]-50]6

Curtiss O. Davis

Jet Propulsion Laboratory
California Institute of Oceanography
4800 Oak Grove Blvd.
Pasadena, CA 91109

ABSTRACT

According to Kirk's as well as Morel and Gentili 's Monte Carlo simulations, the popular simple expression, $R \approx 0.33 b_b/a$, relating subsurface irradiance reflectance (R) to the ratio of the backscattering coefficient (b_b) to absorption coefficient (a), is not valid for $b_b/a > 0.25$. This means that it may no longer be valid for values of remote-sensing reflectance (above-surface ratio of water-leaving radiance to downwelling irradiance) where $R_{rs} > 0.0]$. Since there has been no simple R_s expression developed for very turbid waters, we developed one based in part on Monte Carlo simulations and empirical adjustments to an R_{rs} model and applied it to rather turbid coastal waters near Tampa Bay to evaluate its utility for unmixing the optical components affecting the water-leaving radiance. With the high spectral (10nm) and spatial ($20m^2$) resolution of Airborne Visible-InfraRed Imaging Spectrometer (AVIRIS) data, the water depth and bottom type were deduced using the model for shallow waters. Bottom types included sand, grass flats, and emergent vegetation, with a variety of levels of wave and current-induced suspended sediments apparent in the imagery. It also included turbid water in a deep ship channel that had been scoured off an adjacent shoal region, creating the appearance of a "false" bottom at about 1.5m. This research demonstrates the necessity of further research to improve interpretations of scenes with highly variable turbid waters, and it emphasizes the utility of high spectral-resolution data as from AVIRIS for better understanding complicated coastal environments such as the west Florida shelf.

1. INTRODUCTION

Models have been developed for use with hyperspectral remote-sensing reflectance data collected just above the air-sea interface for the West Florida Shelf [1,2,3,4]. They respond to variations in pigment, detrital, and gel bstoff absorption, chlorophyll a and gelbstoff fluorescence, water Raman scattering, backscattering by water and particulate, and bottom depth and albedo. To date these models have not been systematically used to interpret hyperspectral data derived from high altitude airborne sensors, which can provide a wide variation in component contributions in a single scene.

AVIRIS (Airborne Visible-InfraRed Imaging Spectrometer) is a test bed for future spacecraft imaging spectrometers that may be in orbit in the next century. AVIRIS was

designed largely for terrestrial applications requiring high spectral (10nm) and spatial ($20m^2$) resolutions. It has 224 spectral channels from400 to 2400nm, 20m square pixels when viewing the Earth from 65,000 feet altitude, and it had about 10-20% of the signal-to-noise (S/N) of the Coastal Zone Color Scanner (CZCS) in 1990, when the data reported were acquired. For coastal ocean applications much larger signals are typical compared to those offshore. Thus, adequate signal levels for many nearshore applications can be achieved by binning 25 to 100 pixels together[5].

In March 1990, AVIRIS data were collected from a NASA ER-2 aircraft flying at 65,000 feet altitude on two SW-NE flight lines across the West Florida Shelf and into the mouth of Tampa Bay. These lines were flown at about 1515 Eastern Standard lime and a total of 16 scenes were collected.

The AVIRIS preflight calibration was adjusted to be consistent with the in-flight performance of the instruments. The recalibrated data, representing total radiance at the sensor, was then partitioned into atmospheric path radiance and radiance upwelled from beneath the water surface[5] (water-leaving radiance).

The water-leaving radiance values collected on a windy day near the mouth of Tampa Bay by AVIRIS were very bright, with the maximum remote-sensing reflectance R_{rs} values (the ratio of the water-leaving radiance to the downwelling irradiance) of about 0.035 $ster^{-1}$ (symbols used in this text are listed in Table 1), even for the deep ship channels. In general, maximum R_{rs} value for open ocean stations range from about 0,005 to 0.01 $ster^{-1}$. The high R_{rs} values for the Bay at the time of the study suggest that the bottom depth was very shallow or the water was very turbid due to the high winds and tidal currents. Ibis enigma can be better understood by modeling the R_{rs} spectra.

2. MODEL DEVELOPMENT

Remote sensing reflectance R_{rs} is defined as the ratio of the above surface water-leaving radiance $L_w(0^+)$ to downwelling irradiance $E_d(0^+)$, so

$$R_{rs}=\frac{L_w(0^+)}{E_d(0^+)} \tag{1}$$

and

$$R_{rs}=0.533\frac{R}{Q} \tag{2}$$

where $R=E_u(0^-)/E_d(0^-)$ is the subsurface irradiance reflectance, 0.533 comes from the air-sea interface effect[6], and $Q=E_u(0^-)/L_u(0^-)$ is the so called "Q factor", which is reported in the range of 3 to 12[1,8].

For homogeneous, deep water, Kirk[9] as well as Morel and Gentili[10] simplified R by using Monte Carlo simulations, where b_b is the total backscattering coefficient (a sum of backscattering coefficients from molecules b_{bm} and particulates b_{bp}), a is the total absorption coefficient (a sum of absorption coefficients of water a_w,

$$R=f\frac{b_b}{a} \tag{3}$$

particulate and gelbstoff a_g). The parameter $f \approx 0.33$ for $b_b/a < 0.25$, but f is non-constant for $b_b/a > 0.25$ such that f decreases as b_b/a increases[9,11] and it also increases with increasing sun angle[10]. When $b_b/a > 0.25$, R_{rs} will be > 0.01 ster^{-1}, assuming[3,12,13] a general Q - 3.5. Thus, when R_{rs} is far greater than 0.01 ster^{-1}, f will vary with b_b/a instead of remaining a spectral constant for a given sun angle.

AVIRIS-derived R_{rs} values of Tampa Bay were of order 0.03 ster^{-1} and f was adjusted in a manner consistent with data in Kirk's Fig. 5[9]:

$$f = 0.33\left(1 - \epsilon\frac{b_b}{a}\right) \tag{4}$$

where ϵ is a small constant. Data from Kirk's[9] and Morel and Gentili's[10] Monte Carlo simulations suggest values of ϵ ranging from 0.2 to 0.4. We found a value of $\epsilon \approx 0.33$ worked well for our situation. Then R_{rs} is expressed as

$$R_{rs} \approx 0.176\left(1 - \epsilon\frac{b_b}{a}\right)\frac{b_b}{aQ} \tag{5}$$

which results upon combination of Eqs. 2-4.

Lee et al.[3,4] proposed that b_b/Q can be expressed in the form

$$\frac{b_b}{Q} = \frac{b_{bm}}{Q_m} + X\left(\frac{640}{\lambda}\right)^Y \tag{6}$$

where the final term is an expression for b_{bp}/Q_p. The subscripts "m" and "p" designate molecular and particulate components, respectively.

Thus,

$$b_b = Q\left[\frac{b_{bm}}{Q_m} + X\left(\frac{640}{\lambda}\right)^Y\right] \tag{7}$$

provides an estimate of b_b for use in Eq. 4. If Q is assumed to be equal to about 3.5[3,12,13], then R_{rs} for homogeneous, deep, turbid water is

$$R_{rs} \approx \frac{0.176\left[1 - \frac{1.16}{a}\left(\frac{b_{bm}}{Q_m} + X\left(\frac{640}{\lambda}\right)^Y\right)\right]}{a}\left[\frac{b_{bm}}{Q_m} + X\left(\frac{640}{\lambda}\right)^Y\right] \tag{8}$$

where values for b_{bm} are readily available[14], and Q_m values vary with sun angle[3,4]. For this study, the sun angle was about 49°, so $Q_m \approx 3.9$ is used[3,4].

Due to the shallow water depth in coastal waters, the water-leaving radiance L_w can in general be expressed as a sum of two components: L_{col} from the scattering and attenuation of molecules and particles in the water column, and L_{bot} is the radiance from the bottom reflection. Since coastal waters can be quite turbid, water Raman

scattering and fluorescencee from colored dissolved organic matter (CDOM) are typically negligible (see lee et al.[3]). For this truncated water column, R_{rs}^{col} is adjusted as

$$R_{rs}^{col} \approx R_{rs}^{deep}[1 - e^{-3.2(a+b_b)H}] \quad (9)$$

where R_{rs}^{deep} comes from [q. 8, and the 3.2 in the exponential term is estimated from $3D_d$ in lee et al.[3]. The $2.7(a+b_b)$ term in Eq. 10 is similarly estimated[3].

The bottom contribution R_{rs}^{bot} is expressed as

$$R_{rs}^{bot} = 0.173\rho e^{-2.7(a+b_b)H} \quad (10)$$

where p is the bottom albedo, and H the bottom depth.

For the purpose of modeling and unmixing the spectral components contributing to the R_{rs} curves measured by AVIRIS, X,Y,ρ,H and a must be derived. To determine the total absorption coefficient a, a_w is known from Smith and Baker[14], a_g is expressed as

$$a_g = a_g(440)\, e^{-s(\lambda-440)}, \quad (11)$$

and a_p, the particle absorption coefficient is calculated as $a_p^* * [C]$, where a_p is a pigment-specific absorption curve, typical to the region. Two Parameters $a_g(440)$ and $a_p(440)$ are used to adjust the levels-of a_g and a_p in the model by using measured curve shapes consistent with those involved in the study area. Also the bottom depth H and bottom albedo p must be estimated to model R_{rs}^{bot}. This means, at least six parameters are needed to accomplish the unmixing if the spectral dependencies of a_p, a_g, and p are known.

The study region imaged by AVIRIS is shown in Figures 1 and 2, and it consists of the elbow of Mullet Key (right edge) and Egmont Key, with Egmont Channel (20-30m depth) separating them, The small boxes (see Figure 2) on the image include: (1) a protected shallow grass-flat surrounded by Mullet Key; (2) a mangrove swamp; (3) a deep, turbid channel; (4) a long needle pine forest on Egmont Key; (5) a shallow, turbid region; and (6-7) deeper areas with high wave energy. Also an offshore, clearer location is included, Note that the relatively straight coastlines of Egmont Key were distorted by aircraft roll, also geometric rectification has been applied to the image.

Remote-sensing reflectance spectra averaged over the pixels ineach of the boxed regions are displayed in Figure 3. Here, the bright, infrared signals from the mangrove swamp and long needle pine forest dominated the spectra. The low values in the visible part of the spectrum illustrate how dark the reflectance are for heavy canopies and the offshore waters for the blue part of the spectrum relative to those often observed in terrestrial research. Note the similarity in the visible band between the shallow, sea-grass spectrum and that of either the pine forest or the mangrove canopy. Note also that offshore spectra are much smaller than those near the bay mouth area, especially for the high-energy, turbid conditions during this study. Thus, while these brighter coastal regions appear to be adequately characterized by averaging 100 to 900 pixels per bin to improve signal-to-noise, as many as 2,500 to 10,000 pixels were averaged for dark offshore waters[5]. Note that significant improvements in 1992 AVIRIS performance

have reduced the binning requirements for recently acquired (November 1992) coastal scenes to as few as 25 pixels.

Even with pixel-binning, there remain some irregularities in the spectra due to in part to coherent noise in 1990 AVIRIS scenes (Hamilton et al[15]) and low signal-to-noise ratios. Recent improvement in AVIRIS performance have also eliminated coherent noise effects, Because of residual noise in the 1990 no attempt was made to model R_{rs} spectral curves for wavelengths shorter than 420nm or longer than 680nm.

3. MODEL INTERPRETATIONS

Field data collected by sampling from the R/V Bellows[5] indicate that the slopes of the spectral semi logarithmic line describing a_g for the Bay mouth area is about $0.013nm^{-1}$ (see Eq.1] and Figure 4), and the shapes of the particle absorption spectra can be represented by the curve in Figure 4. Shapes for the albedo curves used in the model for sand and grass bottoms are shown in Figure 5.

Contributions due to a_p, a_g, and ρ were modified by varying $a_g(440)$, $a_p(440)$ and $\rho(500)$ and used in the R_{rs} model for the various study sites. Table 2 and Figures 6-11 show the model parameters and results for the selected locations. Rather good agreement between the measured and the modeled R_{rs} curves was found with a general discrepancy of less than 5%, lhis difference derives from the combination of errors associated with atmosphere correction, a_p and p curves, model parametrization, and noise in the AVIRIS data.

The model parameters used for the offshore location (Fig.6) are similar to those used for modeling offshore R_{rs} curves measured from a ship with a small difference in Y likely due to a -2-hour time difference between ship and AVIRIS measurements. For location 1 (Figure 7), which is inside the elbow of Mullet Key, a spectrally composited bottom albedo (see Figure 5) was used to simulate bottom albedos containing a mixture of pixels containing both sea grass and sand bottom within the sample box of an AVIRIS image. The derived bottom depth is close to the depth for that site from the NOM bathymetric chart (#11414). Also the higher values for $a_p(440)$ and $a_g(440)$ and the lower values for X and $\rho(500)$ for this site compared to those from the more energy-rich Egmont channel area result from a smaller impact of resuspended sediments on the backscattering coefficient in the protected area of the elbow of Mullet Key.

For locations 3 and 5 (see Figures 8 and 9), the AVIRIS-derived R_{rs} curves look very similar, as do the derived parameters (see Figure 3 and Table 2). But from the chart, location 3 is in the Egmont ship channel, with a bottom depth of ~15m, while location 5 is close to Egmont Key with a water depth of ~1.5m. An explanation for this dichotornymay be that wave-induced erosion and currents scoured the sediments off the shoal area north of the channel and transported them over the channel, where they began to settle. This could have made the optically-averaged water-leaving radiance appear to be from a shallow water column of ~1.4m. Without ship data to confirm this speculation, model values for location 5 will be only used to illustrate the uncertainties involved for optically structured water column.

The Tampa Bay mouth region (location 3,5,6, and 7) has about 2-8 times greater $a_p(440)$ and $a_g(440)$, and 10-70 times higher X values than the offshore area. Since X is largely affected by changes in scattering, it suggests that the brighter image of the mouth area is due to large concentrations of suspended particles, and is not

entirely due to the effects of radiance reflected from the bottom .

The derived H_{mod} for this region was within 20% of the NOAA Chart depth, and most model depths were within 10% of the chart depth. The differences may have resulted from errors in the atmospheric correction, uncertainty in the a_w (the accuracy of a_w is about $\pm 10\%$[14]), or perhaps due to vertical inhomogeneity in the suspended particles in the water column.

For the optically deep locations (except location 3), we found that the proposed R_{rs} expression worked well for the turbid waters of this region, Further study, however, with corroborating ship-derived data is needed to better confirm this observation,

4. SUMMARY

1. Careful removal of atmospheric effects and vicarious recalibration of AVIRIS yields spectral R_{rs} curves which can be modeled using mixtures of optical contributions from various components: water molecules, CDOM, suspended particles, and the sea bottom,

2. For the turbid regions for which R_{rs} model curves were derived, the reflectance was nonlinear with b_b/a, e.g. $R \approx 0.33(1-eb_b/a)b_b/a$, and an e value of 0.33 worked well for the model in our study area.

3. Close agreement between curves for AVIRIS-derived R_{rs} and modeled R_{rs} was found for a complex, coastal environment, with most derived water column depth values found to be within about 10% of charted depths for the shallow locations.

4. lhe high X values found at the mouth of lampa Bay suggest that backscattering from suspended particles contributed significantly to the remote-sensing reflectance values determined there.

5. lhe deep location in Egmont channel (location 3) provided an R_{rs} curve similar to that expected for shallow water (e.g. see location 5). One explanation for this may be that a "false bottom" reflectance from suspended sediments scoured from the adjacent shoal region to the north formed at about 1.5m below the surface. The model depends upon an assumption of vertical homogeneity in water-column properties, which was likely violated for this location.

6. As one might expect, R_{rs} curves for shallow sea grass beds were nearly identical to those for emergent vegetation for wavelengths shorter than about 580nm.

5. ACKNOWLEDGEMENT

Special thanks to Robert Steward, Thomas Peacock, David Costello, and Lisa Young for their help in laboratory analyses. Financial support was provided by the National Aeronautics and Space Administration to the University of South Florida (USF) through grant NAGW-465, GSFC contract NAS5-30779, and JPL contract 958914 (RE-198), and by the Office of Naval Research through grant NOOO14-89-J-1091 to USF. Ship support was provided by the State of Florida through the Florida Institute of Oceanography.

Table 1. Symbols and units

$L_w(0^+)$	= surface leaving radiance from water or emergent plants, $Wm^{-2}ster^{-1}$
L_{col}	= radiance from water column, $Wm^{-2}ster^{-1}$
L_{bot}	= radiance from bottom reflectance, $Wm^{-2}ster^{-1}$
$L_w(0^-)$	= subsurface upwelling radiance, $Wm^{-2}ster^{-1}$
$E_u(0^-)$	= subsurface upwelling irradiance, Wm^{-2}
$E_d(0^-)$	= subsurface downwelling irradiance, Wm^{-2}
$E_d(0^+)$	= above surface downwelling irradiance, Wm^{-2}
R_{rs}	= remote sensing reflectance, $ster^{-1}$
R	= irradiance reflectance
a	= absorption coefficient, m^{-1}
b_b	= backscattering coefficient, m^{-1}
ρ	= bottom albedo
H	= water depth, m
Q	= ratio of upwelling irradiance to radiance, ster
s	= spectral slope parameter (rim-l)

Table 2. R_{rs} mode' parameters used to fit the data for locations shown in Figure 2.

Locations	$a_p(440)$	$a_g(440)$	X	Y	$\rho(500)$	H_{mod}	H_{mea}
offshore	0.036	0.037	0.00086	1.8	0.50	25.0	24.7
#l	0.206	0.320	0.008	0	0.08	1.1	0.9
#3	0.152	0.033	0.017	0	0.14	1.4	15
#5	0.195	0.070	0.021	0	0.15	1.3	1.5
#6	0.137	0.100	0,035	0			10
#7	0.290	0.170	0.055	0			3.3

Note: H_{mea} comes from Chart #11414 of NOAA. Where the location has no $\rho(500)$ and H_{mod} means it can be seen as optically deep water.

6. References

1. Carder, K.L. and R.G. Steward, 1985, "A remote sensing reflectance model of a red tide dinoflagellate off West Florida," *Limnol. Oceanogr. 30(2), 286-298.*

2. Carder, K.L., R.G. Steward, J.H. Paul and G.A. Vargo, 1986, "Relationships between chlorophyll and ocean color constituents as they affect remote sensing reflectance models, " *Limnol. Oceanogr. 31(2), 403-413.*

3, Lee, Z.P., K.L. Carder, S.K. Hawes, R.G. Steward, T.G. Peacock and C.O. Davis, 1992, "An interpretation of high spectral resolution remote sensing reflectance", *Optics of the Air-Sea Interface,* Proc. SPIE, Vol. 1749, 49-64,

4, Lee, Z.P., K.L. Carder, S.K. Hawes, R.G. Steward, T.G. Peacock and C.O. Davis, 1993, "A Model for Interpretation of Hyperspectral Remote Sensing Reflectance", *Appl. Optics,* submitted.

5. Carder, K.L., P. Reinersman, R.G. Steward, R.F. Chen, F. Muller-Karger, C.O. Davis, and M. Hamilton, 1993, "AVIRIS Calibration and Application in Coastal Oceanic Environments," *Remote Sensing of the environment,* Special Issue on Imaging Spectrometry (G. Vane, editor), in press.

6. Austin, R.W., 1974, "Inherent spectral radiance signatures of the ocean surface," *Ocean Color Analysis, S10* Ref. 7410, April.

7. Austin, R.W., 1979, "Coastal zone color scanner radiometry", *Ocean Optics VI*, Proc. SPIE. 208. 170-177,

8. Gordon, Ii.'R., R.C. Smith, and J.R.V. Zaneveld, 1979, "Introduction to Ocean Optics, " *Ocean Optics VI*, Proc. SPIE. 208, 15-63.

9. Kirk, J.T.O., 1991, "Volume scattering function, average cosines, and the underwater light field," *Limnol. Oceanogr. 36(3), 455-467.*

10. Morel, A. and B. Gentili, 1991, "Diffuse reflectance of oceanic waters: its dependence on sun angle as influenced by the molecular scattering contribution", *Appl. Optics 30, 4427-4438.*

11. Jerome, J.H., R.P. Bukata and J.E. Bruton, 1988, "Utilizing the components of vector irradiance to estimate the scalar irradiance in natural waters," *Appl. Optics 27(19), 4012-4018.*

12. Gordon, H,R., O.B. Brown and M.M. Jacobs, 1975, "Computed relationship between the inherent and apparent optical properties of a flat homogeneous ocean," *Appl. Optics 14,' 417-427.*

13. Gordon, H.R., O.B. Brown, R.H. Evans, J.W. Brown, R.C. Smith, K.S. Baker, and D.K. Clark, 1988," A Semianalytic Radiance Model of Ocean Color", *J. Geophys. Res. 93(D9), 10,909-10,924.*

14. Smith, R. C. and K.S. Baker, 1981, "Optical properties of the clearest natural waters," *Appl. Optics 20(2), 177-184.*

15. Hamilton, M., C.O. Davis, S.H. Pilorz, W.J. Rhea, and K.L. Carder, 1991, "Examin ationofChlorophyll Distribution in Lake Tahoe, Using the Airborne Visible and Infrared Imaging Spectrometer (AVIRIS), *Proceedings of the Third AVIRIS Workshop*, JPL Pub. , No. 91-28.

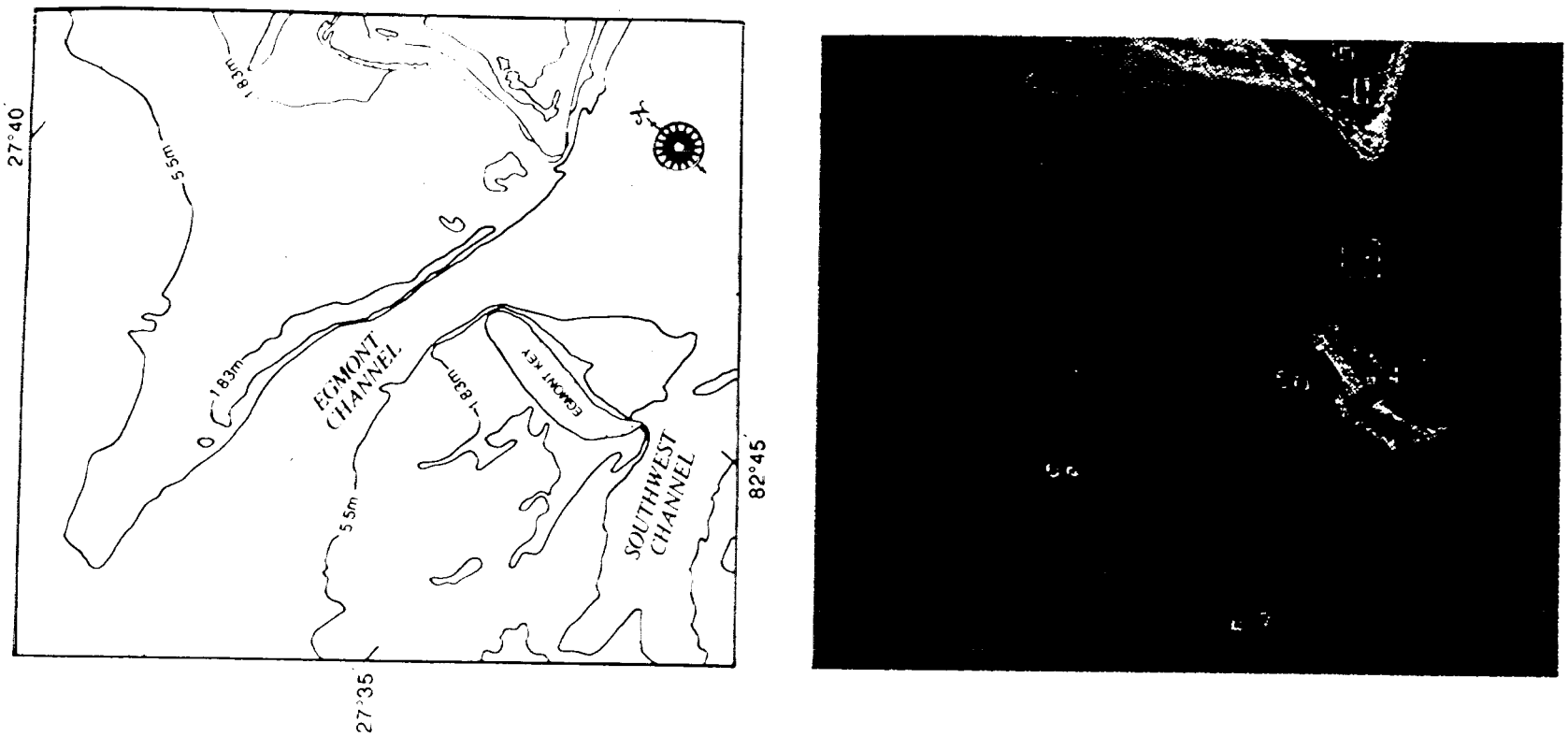

Fig 1. Schematic of the bathymetry for the mouth of Tampa Bay

Fig. 2. Atmospherically corrected image from AVIRIS of the mouth of Tampa Bay, composited using bands centered at 445, 555, and 675nm with band widths of about 9 6nm. the numbered boxes locate the sites where R_{rs} spectra were determined for discussion in the text. Note that turbidity may be hiding many of the bottom features.

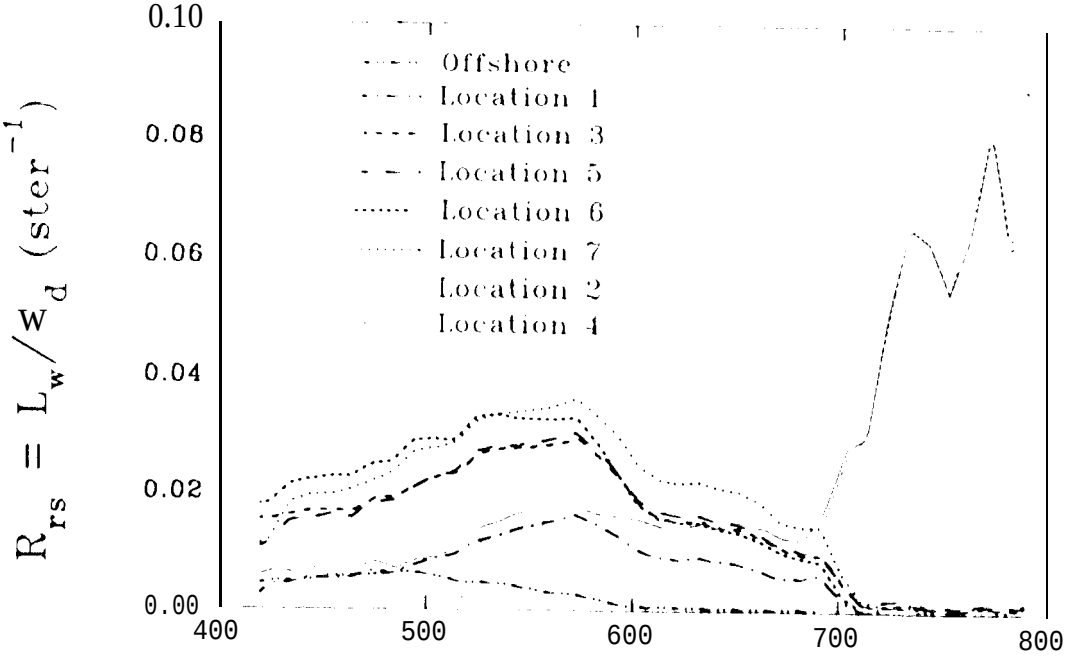

Fig. 3. R_{rs} spectral curves for sites shown on Figure 2. Note that locations 2 and 4 contain emergent mangroves and pines, respectively, and location 1 contains a sea grass bed, protected from waves by Mullet Key.

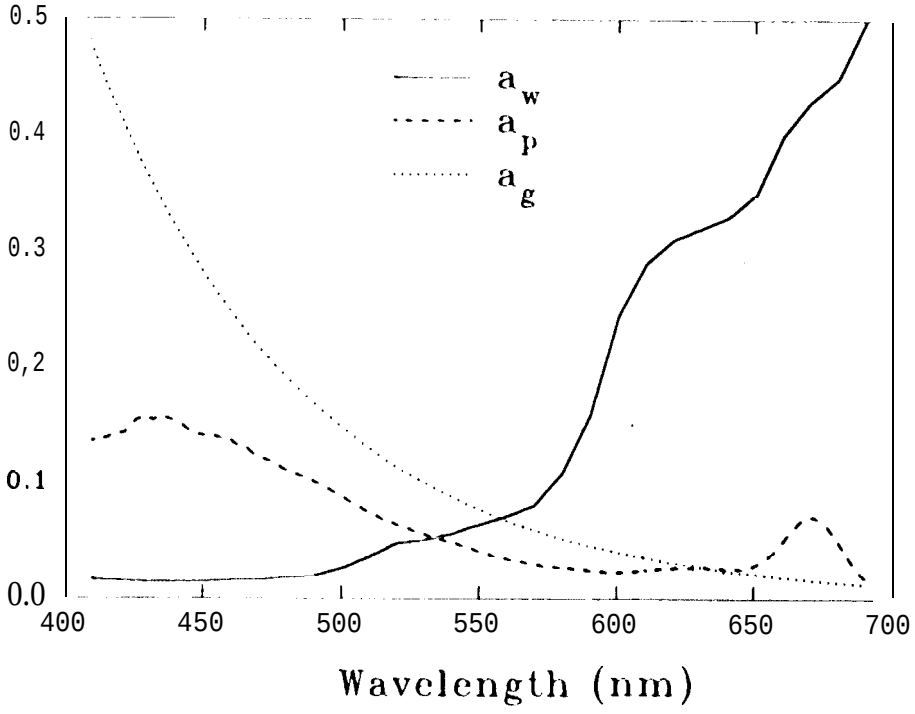

Fig. 4. Absorption spectral shapes for pure water, particles, and gelbstoff or CDOM .

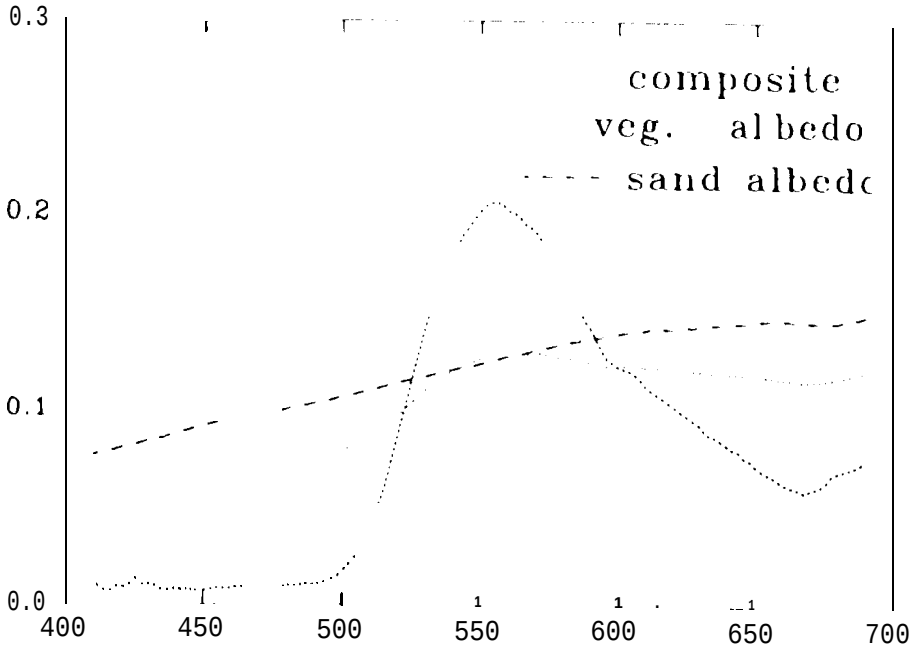

Fig. 5. Bottom albedo spectra for sand and grass bottoms. Composites can be used for grass beds not completely covering the bottom.

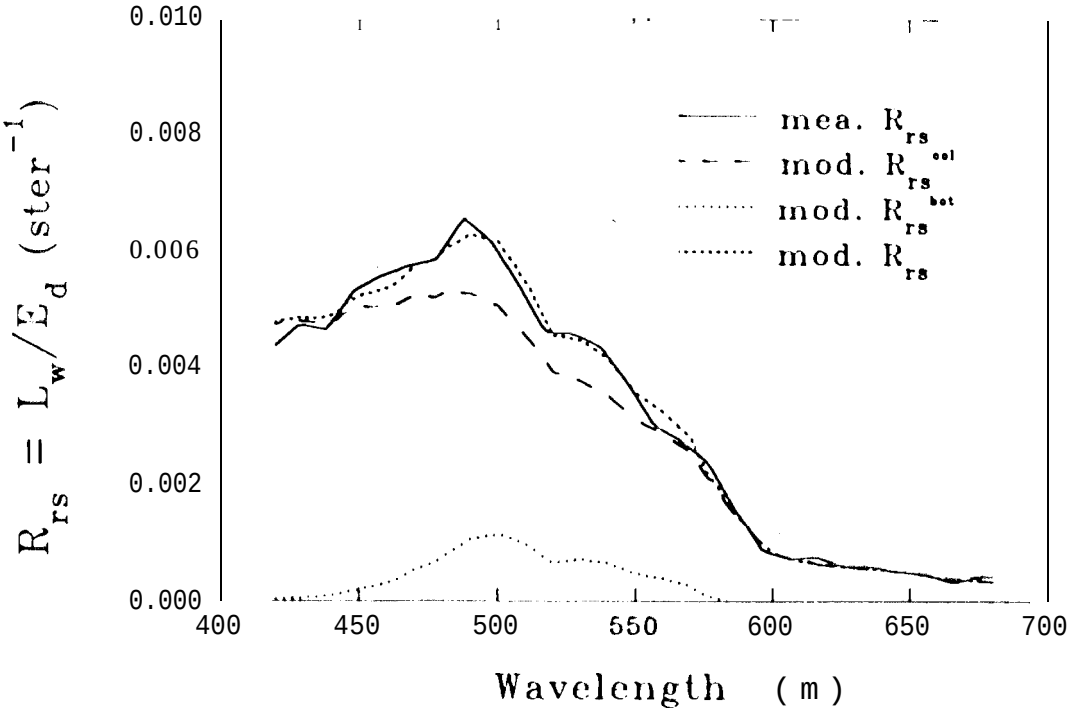

Fig. 6. Spectra for measured and modeled R_{rs} data for an offshore station in 25m of water, Spectra include parts due to the water column.
the bottom and, their sum.

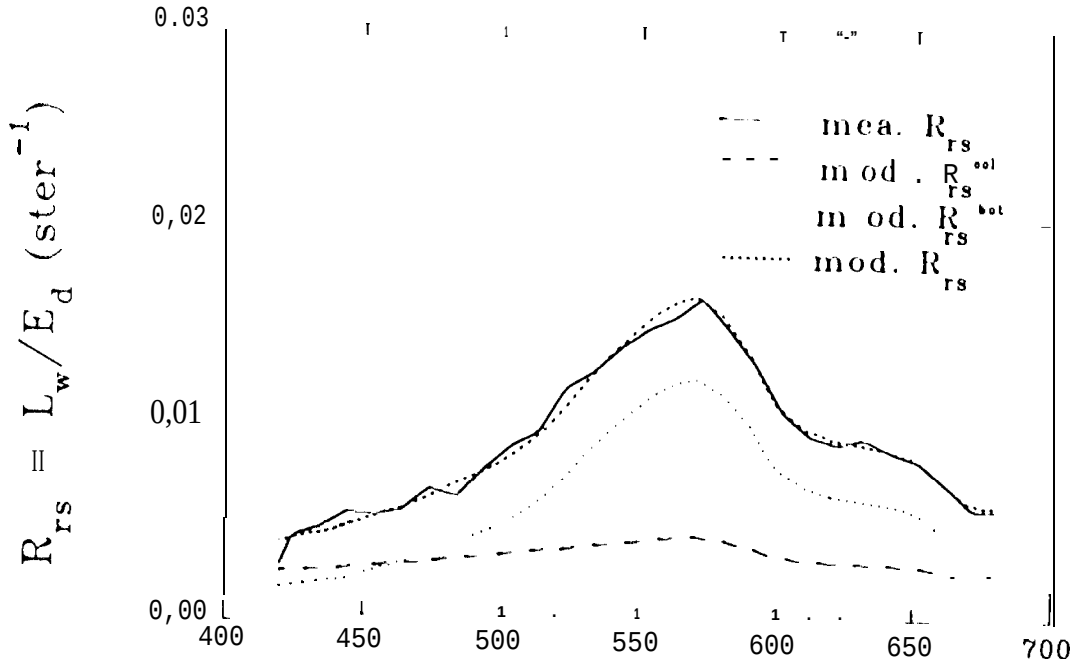

Fig. 7. Spectra for measured and modeled R_{rs} data for a station over a grass bed at location #1.

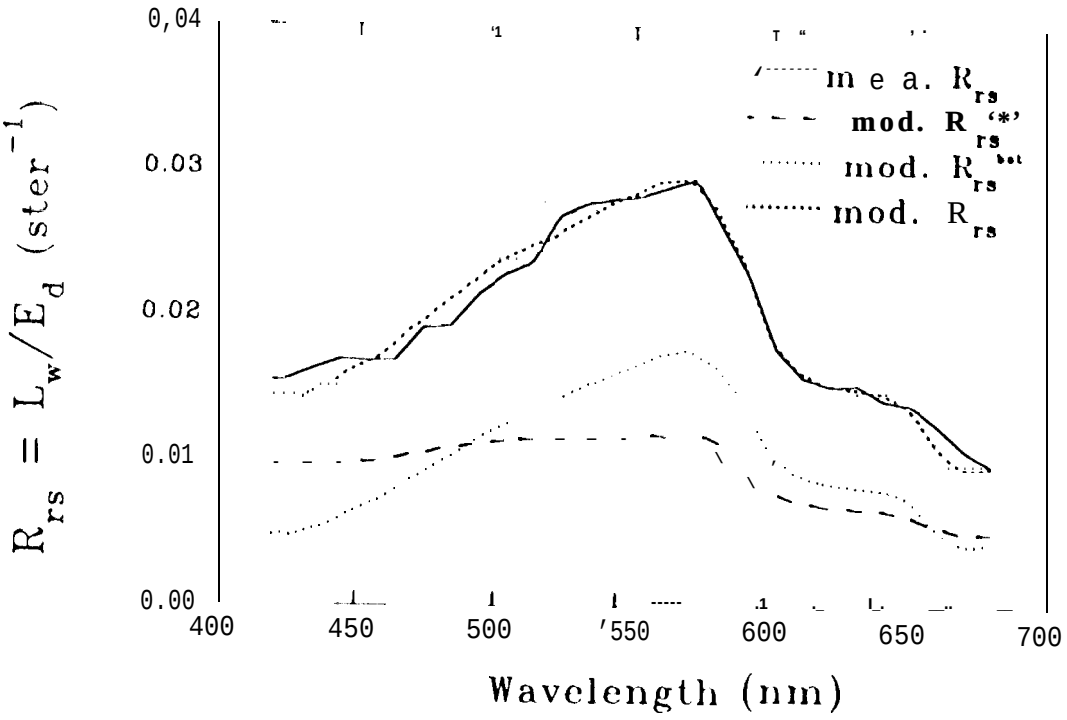

Fig, 8. Spectra for measured and modeled R_{rs} data for a station over the ship channel at location #3.

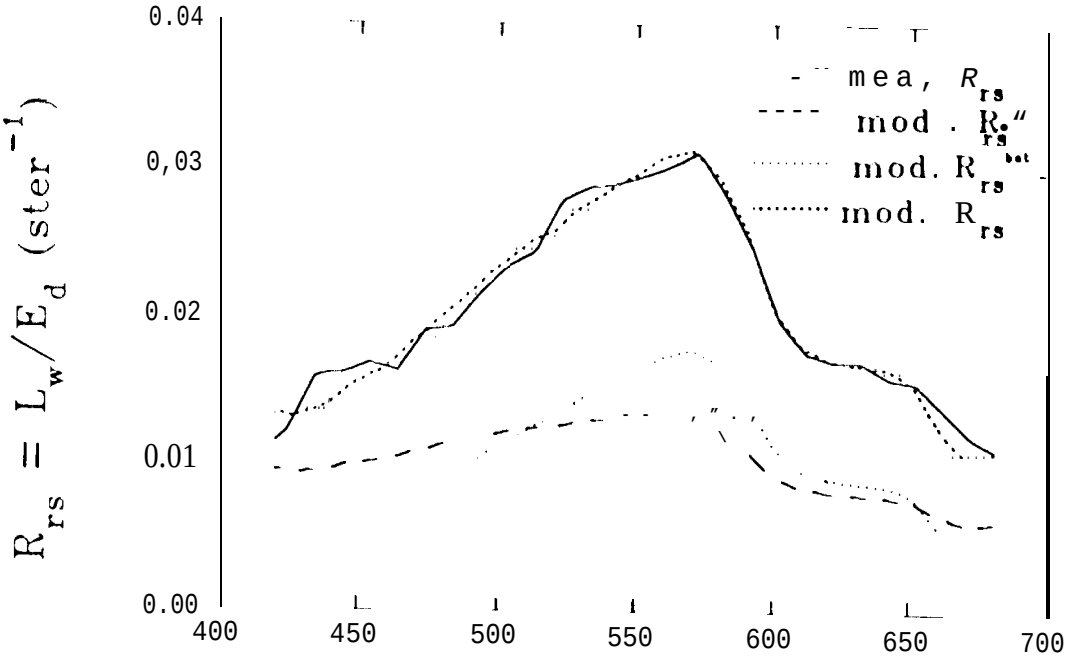

Fig. 9. Spectra for measured and modeled R_{rs} data for a station in the sandy shallow water near Egmont Key at location #5.

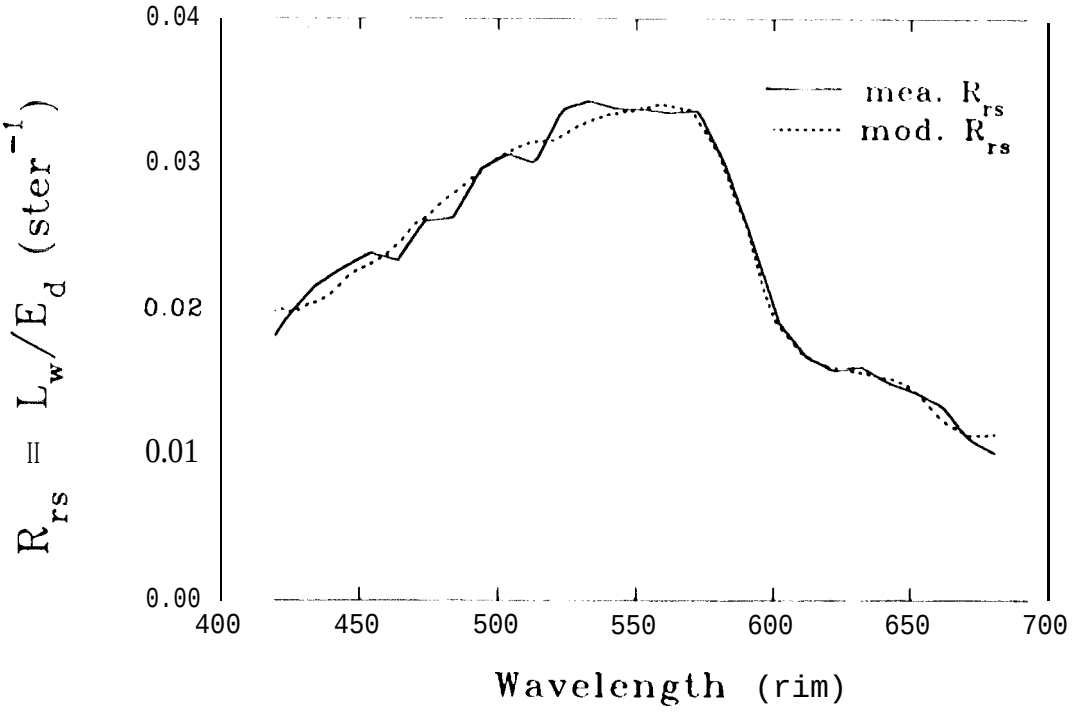

Fig. 10, Spectra for measured and modeled R_{rs} data for a rather turbid station in the nearshore ship channel.

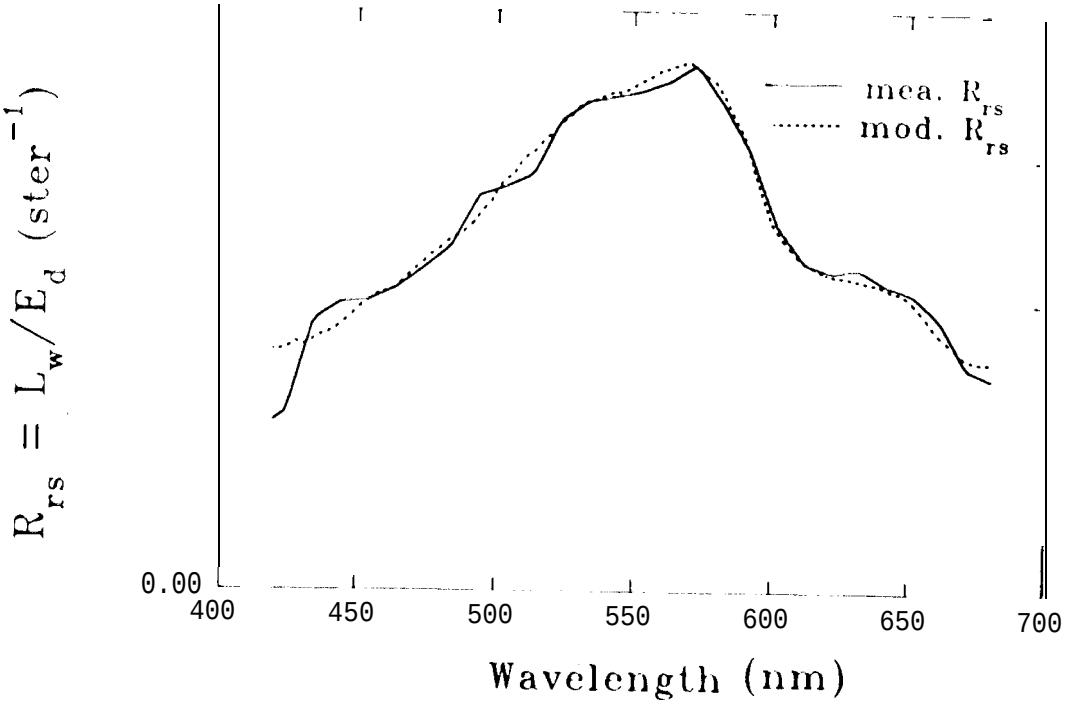

Fig. 11. Spectra for measured and modeled R_{rs} data for very turbid station near the ship channel.